JACS
JOURNAL OF THE AMERICAN CHEMICAL SOCIETY

Article

pubs.acs.org/JACS

Size-Dependent Excited State Behavior of Glutathione-Capped Gold Clusters and Their Light-Harvesting Capacity

Kevin G. Stamplecoskie and Prashant V. Kamat*

Notre Dame Radiation Laboratory, Department of Chemistry and Biochemistry, University of Notre Dame Notre Dame, Indiana 46556, United States

Supporting Information

ABSTRACT: Glutathione-protected gold clusters exhibit size-dependent excited state and electron transfer properties. Larger-size clusters (e.g., $Au_{25}GSH_{18}$) with core-metal atoms display rapid (<1 ps) as well as slower relaxation (~200 ns) while homoleptic clusters (e.g., $Au_{10-12}GSH_{10-12}$) exhibit only slower relaxation. These decay components have been identified as metal−metal transition and ligand-to-metal charge transfer, respectively. The short lifetime relaxation component becomes less dominant as the size of the gold cluster decreases. The long-lived excited state and ability to participate in electron transfer are integral for these clusters to serve as light-harvesting antennae. A strong correlation between the ligand-to-metal charge-transfer excited state lifetime and photocatalytic activity was evidenced from the electron transfer to methyl viologen. The photoactivity of these metal clusters shows increasing photocatalytic reduction yield (0.05−0.14) with decreasing cluster size, Au_{25} < Au_{18} < Au_{15} < Au_{10-12}. Gold clusters, $Au_{18}GSH_{14}$, were found to have the highest potential as a photosensitizer on the basis of the quantum yield of electron transfer and good visible light absorption properties.

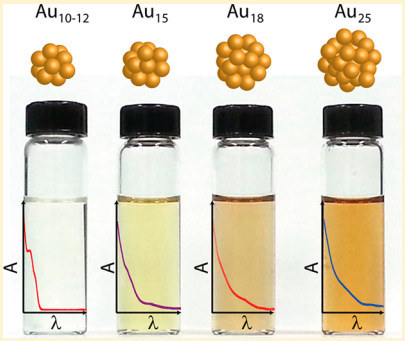

INTRODUCTION

Metal clusters are a new class of optically active nanomaterials, which exhibit interesting photophysical properties.[1−6] In particular, thiol-protected gold clusters (Au_x−RS_y) have received a lot of attention in recent years for their size-dependent, excited state properties.[7−14] These metal clusters display optical properties with molecule-like transitions that are very different from those of their larger nanoparticle cousins.[1,12,15−21] These atomically precise clusters provide an important link between metal nanoparticles and single atoms. Metal nanoparticles display visible light absorbance due to plasmon excitation, which has become well understood and exploited in various applications like surface enhance Raman spectroscopy, over the past couple of decades. Below a certain size, nanoparticles no longer support plasmon absorptions but transition to something more like molecular optical properties.[17,22] Furthermore, ultrafast relaxation processes discovered by Goodson et al. suggest that these tiny particles are not entirely like molecules but are an all-new class of organo-metallic light absorbers.[1,23] The structure as well as optical and electronic properties of atomically precise clusters varies greatly with the exact metal atom number as well as the nature of the coordinating ligands. Many gold clusters have been isolated that follow a "magic number" that corresponds to exact atom and ligand numbers with particular electronic stability, such as $Au_{25}RS_{18}$, which also have spherical geometry due to the bond structure. Other clusters, however, such as the homoleptic clusters discussed herein ($Au_{10-12}RS_{10-12}$) and $Au_{38}(SR)_{24}$ can be isolated despite the fact that they do not follow the magic number rule and do not form a spherical geometry.[22]

Various Au_x−RS_y have recently been investigated in light-harvesting applications like water splitting[24] and solar cells.[25,26] The number of metal atoms, metal atom-to-thiol coordinating ligand ratio (Au/RS), and oxidation state of the metal core have all been shown to have dramatic effects on the absorption and emission properties.[1,9,22,27−31] The same variations in cluster composition can significantly affect the photocatalytic activity of these clusters in light-harvesting applications.

Few ultrafast transient absorption spectroscopy studies have reported the excited state behavior of $Au_{25}RS_{18}$ clusters.[1,15,32] In our previous study we have characterized the excited state of glutathione-stabilized gold clusters with an emission maximum at 600 nm and a lifetime of 780 ns.[11] Such a long-lived excited state arising from the ligand-to-metal charge transfer state allowed us to sensitize TiO_2 and design a photoelectrochemical cell with 2% efficiency and photocatalytic hydrogen generation.

The above referred studies lead to the question whether one can modulate the excited state properties by varying the metal cluster size. Herein we use ultrafast (femtosecond) transient absorption spectroscopy (fsTAS) and nanosecond transient absorption spectroscopy (nsTAS) to investigate the excited state behavior of glutathione-protected clusters; $Au_{25}GSH_{18}$, $Au_{18}GSH_{14}$, $Au_{15}GSH_{13}$, and $Au_{10-12}GSH_{10-12}$. By employing methyl viologen (MV^{2+}) as a probe molecule we have succeeded in determining the quantum yield ($\Phi_{e\text{-}T}$) of electron transfer between excited metal clusters and MV^{2+} and establish the size-dependent properties.

Received: May 28, 2014
Published: July 17, 2014

   dx.doi.org/10.1021/ja505361n | J. Am. Chem. Soc. 2014, 136, 11093−11099

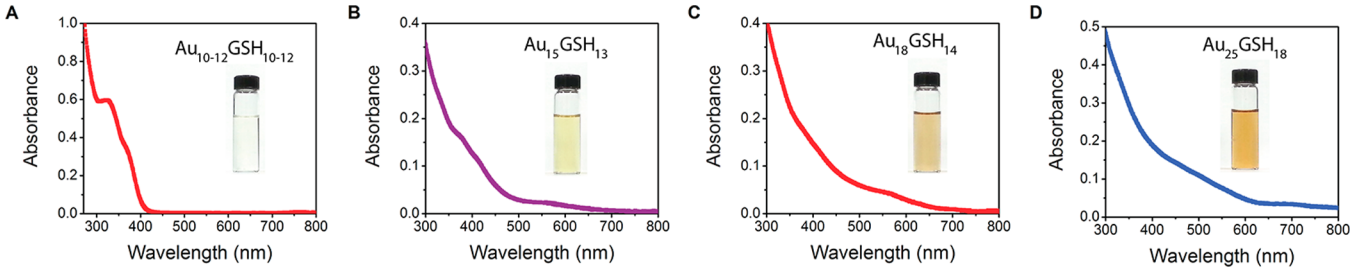

Figure 1. Absorption spectra of metal clusters of different sizes prepared by varying the pH and reduction with CO (A) pH 7, (B) pH 9, (C) pH 10, and (D) pH 11 solutions. The inset in each frame is an image of a vial containing each of the solutions corresponding to the individual metal clusters.

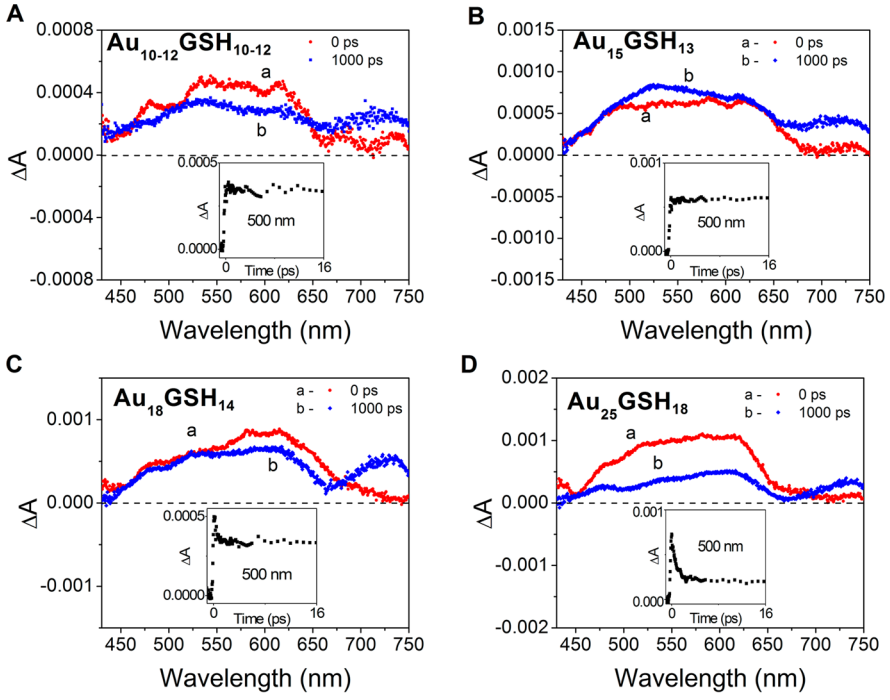

Figure 2. Difference absorbance spectra recorded immediately and 1 ns after 387 nm femtosecond excitation of deaerated aqueous solution containing (A) $Au_{25}GSH_{18}$, (B), $Au_{18}GSH_{14}$ (C), $Au_{15}GSH_{13}$, and (D) $Au_{10-12}GSH_{10-12}$. Insets show absorption−time profiles recorded at 500 nm.

GLUTATHIONE-PROTECTED AU CLUSTERS WITH VARYING SIZE

The synthesis of different sizes of thiolated gold clusters (Au_xGSH_y) was based on a previously reported methodology.[7] Briefly, 110 mL aqueous solutions of 2.5 mM L-glutathione (≥98.0%) and 1 mM HAuCl4·3H_2O (≥99.9%) were maintained at a controlled pH under CO atmosphere. The pH of the solution was adjusted to 11, 10, 9, and 7 using 1 mM aqueous sodium hydroxide to obtain $Au_{10-12}GSH_{10-12}$, $Au_{15}GSH_{13}$, $Au_{18}GSH_{14}$, and $Au_{25}GSH_{18}$, respectively. The smallest of these clusters are the $Au_{10-12}GSH_{10-12}$, which are "homoleptic", which means that they have the same number of metal atoms as ligands. Further characterization of these clusters has been reported previously.[7]

The solutions turned from yellow to clear within minutes of mixing the precursors, indicating the formation of a Au(I)−glutathione complex.[7,30] The mixtures were then purged with CO for 2 min and sealed with 1 bar of CO as a reducing agent and stirred for 24 h. The clear solutions turned to light yellow or brown, depending upon the pH of the medium. The difference in solution color can be readily visualized as shown in the insets of Figure 1.

The absorption spectra of these clusters (Figure 1) matched with those reported for $Au_{10-12}GSH_{10-12}$ $Au_{15}GSH_{13}$, $Au_{18}GSH_{14}$, and $Au_{25}GSH_{18}$ in an earlier study and exhibited size-dependent absorption onset.[7] It is interesting to note that the absorption onset for $Au_{10-12}GSH_{10-12}$, the smallest size, is around 400 nm and shifts to the red as the size of the cluster become larger. Both $Au_{15}GSH_{18}$ and $Au_{18}GSH_{14}$ absorb strongly in the visible region, exhibiting absorption onsets at 700 and 800 nm, respectively. As discussed earlier the control of pH (7−11) during CO reduction enables the stabilization of metal clusters of defined size in the range of 10−25 Au atoms. The clusters were further characterized using mass spectrometry (see Figure S6 in the Supporting Information [SI]). While some gold clusters have been reported to have high emission quantum yields,[30] the particles made here have a very little observable emission (see Figure S7 in the SI). These clusters are stable when stored under carbon monoxide and without adjusting the pH. However, when open to the atmosphere, visible color changes can be observed within ∼24 h, and more rapid changes occur (∼1 h) when the pH of the solution is adjusted to more neutral or acid pH.

dx.doi.org/10.1021/ja505361n | J. Am. Chem. Soc. 2014, 136, 11093−11099

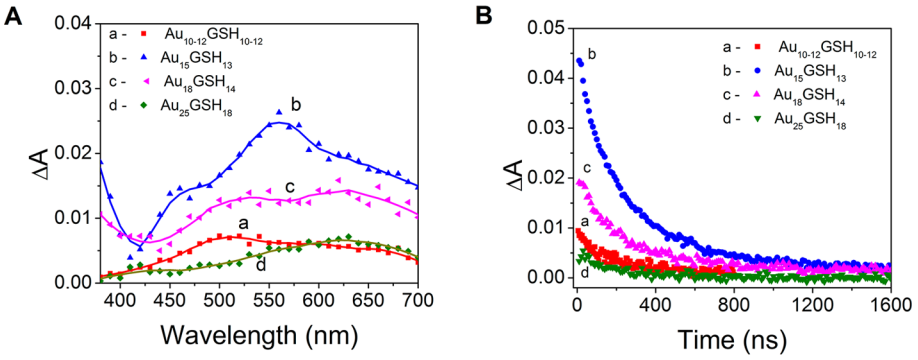

Figure 3. (A) Difference absorbance spectra of excited Au_xGSH_y clusters recorded 100 ns after a 355 nm nanosecond laser pulse excitation of deaerated aqueous solution containing (a) $Au_{10-12}GSH_{10-12}$ (b) $Au_{15}GSH_{13}$, (c) $Au_{18}GSH_{14}$, and (d) $Au_{25}GSH_{18}$. (B) Corresponding absorption decay of excited clusters recorded at 500 nm for each of the cluster solutions.

Table 1. Excited-State Lifetimes of Gold Clusters and Electron Transfer Efficiency

cluster	τ_{fs} (ps)	A_{rfs}	τ_{ns} (ns)	A_{rns}	Φ_{et} (%)
$Au_{10-12}GSH_{10-12}$	N/A	N/A	164 ± 19	1	1.65 ± 0.08
$Au_{15}GSH_{13}$	N/A	N/A	241 ± 5	1	3.97 ± 0.40
$Au_{18}GSH_{14}$	0.37 ± 0.05	0.3	255 ± 45	0.7	4.23 ± 0.23
$Au_{25}GSH_{18}$	0.80 ± 0.03	0.7	203 ± 29	0.3	2.37 ± 0.16

SIZE-DEPENDENT EXCITED STATE PROPERTIES OF AU-GSH

To determine the excited state behavior of each of the glutathione-stabilized gold clusters, the time-dependent change in absorbance (ΔA) of the solutions was monitored after a 387 nm laser pulse (150 fs) excitation (energy density of 20 mW/cm^2 pulsed at 1 kHz). Deaerated samples were placed in a 2 mm path length cuvette for these femtosecond transient absorption measurements. The difference absorption spectra recorded immediately and 1 ns after 387 nm excitation are shown in Figure 2 along with the decay profile at 500 nm (insets) for each of the cluster suspensions.

The appearance of a prompt transient with broad absorption in the visible represents the formation of the excited state. For smaller metal clusters ($Au_{15}GSH_{13}$ and $Au_{10-12}GSH_{10-12}$) the absorption is dominated by a single, long-lived species. For larger clusters ($Au_{25}GSH_{18}$, $Au_{18}GSH_{14}$), however, we see two distinguishable transient features. The presence of excited states with two different lifetimes is consistent with earlier reported characteristics of metal cluster excited state.[1,11,15,32] Additional excited state absorption−time profiles recorded at probe wavelengths, 500 and 650 nm are shown in the SI (Figure S1). It is evident from the excited state decay at 500 nm that there is a dominant excited state relaxation for $Au_{25}GSH_{18}$ that occurs within the first two picoseconds. The fast component of the transient absorption decay can be fit to a monoexponential kinetic expression with a lifetime of 0.80 ± 0.03 ps (see Figure S2 in the SI). This rapid relaxation is followed by a long-lived excited state absorption (>2 ns), which is too long to be resolved in these experiments. The rapid relaxation is also seen for $Au_{18}GSH_{14}$ clusters as well (τ = 0.37 ± 0.05 ps), but to a lesser extent. The short time scale lifetime becomes less prominent with decreasing cluster size and is nonexistent for the smallest clusters.

Interestingly, the short time scale excited state decay is not observable for either $Au_{15}GSH_{13}$ or $Au_{10-12}GSH_{10-12}$. For all four different size clusters, the transient absorption decay profiles at 650 nm (Figure S1 in the SI) show only long-term transient behavior. The absence of a short-lived component at 650 nm selectively provides the kinetic information on the long-lived excited state. Furthermore, comparison of the transient decays at 500 and 650 nm allows us to resolve behavior of short and long-lived excited states.

We further probed the long time component of the excited state deactivation using nanosecond laser flash photolysis. A laser pulse (355 nm, 20 ns fwhm with energy 10 mW and a repetition rate of 10 Hz) was used for excitation. Each sample was diluted to have a matched absorbance of 0.50 at 355 nm (the excitation wavelength, see Figure S3 in the SI). The transient absorption spectrum recorded 50 ns after the laser pulse for each of the cluster solutions is shown in Figure 3A. All these clusters exhibit broad absorption throughout the visible region similar to the one seen in femtosecond transient absorption studies. $Au_{25}GSH_{18}$ clusters show lower absorption than the smaller clusters. Since the short-lived excited state decays within the nanosecond laser pulse duration, the transient absorption signal captures only the contributions from the long-lived excited state.

The absorption−time profiles representing the excited state decay were recorded at 500 nm, and they are shown in Figure 3B. Each of these traces was fit to a biexponential kinetic expression to resolve the longer components of the excited state decay (see Figure S4 in the SI). The analysis showed that the long time component dominated this fraction of the decay. The lifetimes of the long-lived components for all different clusters were in the range of 164−255 ns (see Table 1).

The long-lived component of the excited state (~200 ns) of the metal cluster is attributed to a ligand-to-metal charge-transfer excited state. As discussed earlier, electron transfer from the negatively charged ligands to the electron-accepting gold atoms promotes the formation of the charge-transfer state.[11,15] It is this long-lived excited state that is responsible for the intense near-infrared emission seen for some of these clusters.[1,8,11,30,31] In order to further elucidate the excited state processes we have qualitatively illustrated a molecular orbital picture for the Au_xGSH_y clusters with various electronic transitions (Scheme 1).

dx.doi.org/10.1021/ja505361n | J. Am. Chem. Soc. 2014, 136, 11093−11099

Scheme 1. Energy Level Diagram of Au_xGSH_y Clusters[a]

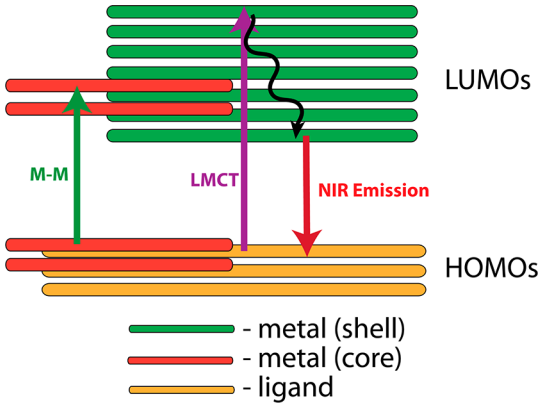

[a]Note that, for homoleptic clusters, there are no metal core states and, therefore, no M−M transitions.

The following experimental and theoretical findings were assembled from the present work and literature to derive the energy diagram in Scheme 1.

1. Metal−metal electronic transitions give rise to steady-state visible absorbance for $Au_{25}GSH_{18}$, $Au_{18}GSH_{14}$ and $Au_{15}GSH_{13}$ clusters (Figure 1).[9,10]
2. Ultraviolet absorbance arises from transitions between molecular orbitals with high ligand contribution to orbitals with high metal character (ligand-to-metal charge transfer).[9,31]
3. A rapid (<1 ps lifetime) decay pathway is seen for excited $Au_{25}GSH_{18}$ and $Au_{18}GSH_{14}$, which have a core of metal atoms.
4. A long-lived (~200 ns lifetime), charge-transfer component is exhibited for all clusters, including homoleptic $Au_{10-12}GSH_{10-12}$.
5. NIR emission in the clusters originates from the charge-transfer excited state.[1,8,11,30,31]

Experimental and theoretical works have shown that Au_{25}, Au_{18}, and Au_{15} have metal cores, whereas Au_{10-12} are polymers of Au−thiol, where all Au atoms are coordinated by thiols (no core).[9,10,28] Ligand-to-metal charge-transfer (LMCT) absorption and NIR emission occur for all clusters, including small homoleptic clusters.[1,8,11,30,31] In Scheme 1, LMCT is a transition favored for all sizes of clusters as characterized from the absorbance <400 nm in Figure 1.[11,15] In contrast to small homoleptic clusters, these larger clusters have a core of metal atoms. Thus, larger clusters with a core−shell structure exhibit additional metal−metal transitions (M−M in Scheme 1). M−M represents metal−metal absorption transitions corresponding to the visible absorbance in Figure 1B, C and D. The rapid relaxation seen in femtosecond transient absorption experiments shows the time scale with which M−M excited state depopulates.

The electronic transitions in smaller, $Au_{10-12}GSH_{10-12}$ homoleptic complexes can be understood by a simplified version of Scheme 1, with no metal−metal-type transitions or metal core states. This property arises from the absence of reduced core metal atoms where each of the atoms is coordinated to at least one glutathione. $Au_{15}GSH_{13}$ clusters have been identified as the smallest clusters that still have a metal core.

There have been few reports investigating the photophysical properties of small metal nanoparticles to understand the transition from gold nanoparticles (AuNP) to molecule-like clusters.[12,17,33] It is important to note that the transitions seen in Au_xGSH_y clusters are different from the plasmonic transitions seen with larger (>5 nm) metal nanoparticles. In contrast to thiolated gold clusters, the AuNP absorption is dominated by an absorbance at ~530 nm arising from the localized surface plasmon resonance.[16,34] The excitation of Au NP gives rise to coherent oscillation of electrons that relax and release the energy as heat. These collisions are called electron−phonon relaxation and occur over ~1 ps period.[35−37]

Looking at the femtosecond transient absorption data of Au_xGSH_y clusters, with increasing contribution of the fast decay component as the cluster size increases, one might argue that we may be observing a transition from molecular complexes to nanomaterials with increasing cluster size. First of all it should be noted that the fast component of the decay of these clusters is different from an electron−phonon relaxation. Second, the transitions in these thiolated gold clusters are molecule-like and are not like those of nanoparticles.[1] One way to distinguish these two processes is to look into the dependence of the decay with varied excitation intensity. The electron−phonon relaxation lifetime in metal nanoparticles is dependent on the excitation power.[36,38] Higher excitation power for AuNP gives rise to hotter particles, which increases the lifetime of the electron−phonon decay. The excited state decay at 500 nm for $Au_{25}GSH_{18}$ at two different laser powers is shown in Figure 4 as

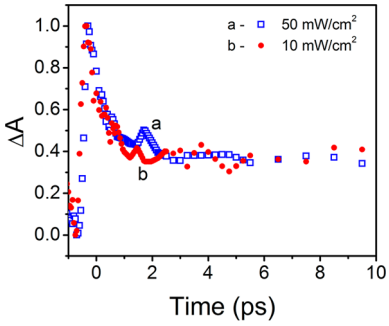

Figure 4. Excited state absorption decay recorded at 500 nm following excitation of $Au_{25}GSH_{18}$ solution with 387 nm laser pulse using two different intensities (a) 50 mW/cm² and (b) 10 mW/cm² The traces are normalized to a maximum *y*-axis value of 1.

well as for a number of different powers in Figure S5 (in the SI). The normalized decay traces in Figure 4 show no observable change in the short lifetime component during the decay. On the basis of these results we can conclude that Au_xGSH_y clusters exclusively exhibit molecular-like properties and do not display plasmonic-type behavior like their larger nanoparticles counterparts.

SIZE-DEPENDENT ELECTRON TRANSFER

Au_x-RS_y clusters have been proposed as a new class of photosensitizers for mesoscopic TiO_2 films and they have been shown to be useful for metal cluster-sensitized solar cells and photocatalytic generation of hydrogen with efficiencies that are comparable to other dyes and semiconductors.[25,26] The optical properties of light-absorbing materials have direct implications in dictating their overall photocatalytic activity. For example, in light-harvesting applications it is often desirable to maximize

dx.doi.org/10.1021/ja505361n | J. Am. Chem. Soc. 2014, 136, 11093−11099

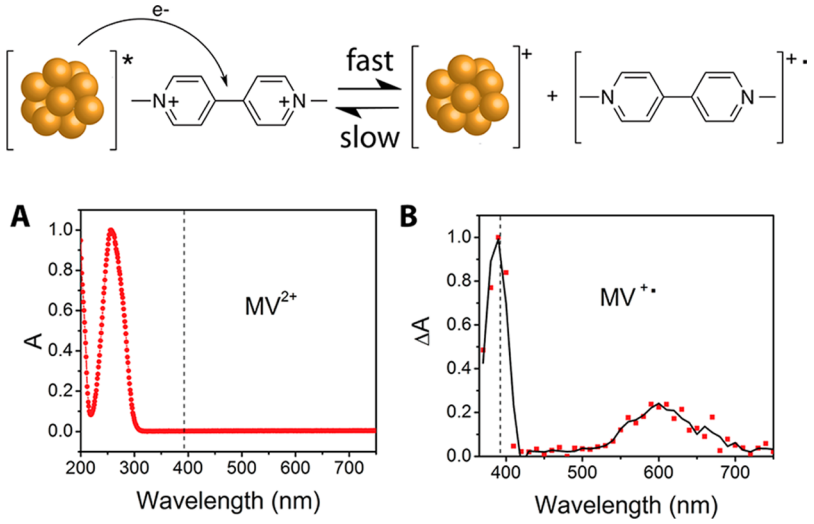

Figure 5. (Top) Schematic illustration of electron transfer from excited gold clusters to MV^{2+}. (A) Absorption spectrum of a 2 mM aqueous MV^{2+} solution in water and (B) Absorption spectrum $MV^{+\bullet}$ recorded 1.5 μs after 355 nm laser pulse excitation of deaerated aqueous $Au_{18}GSH_{14}$ solution containing 70 μM MV^{2+}. Each spectrum was normalized so that the peak absorption was 1. The dashed line at 396 nm in (B) is to indicate the probe wavelength used in determining the quantum efficiency (Φ_{et}) of electron transfer.

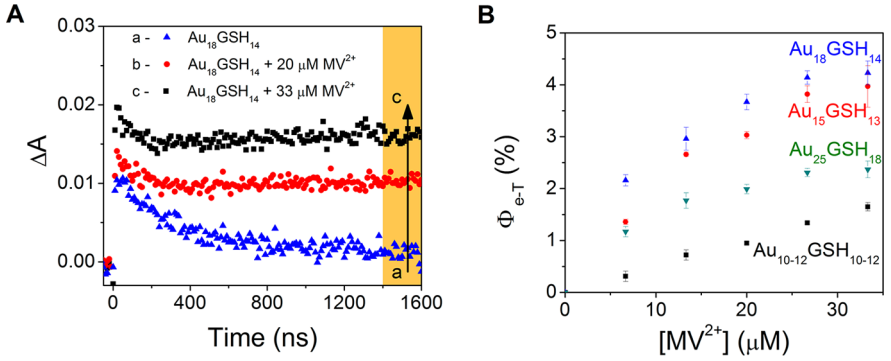

Figure 6. (A) Absorption−time profiles recorded at 396 nm following the 355 nm laser pulse excitation of aqueous $Au_{18}GSH_{14}$ solution containing (a) 0, (b), 20 μM, and (c) 30 μM [MV^{2+}]. (B) Quantum efficiency of electron transfer, Φ_{et}, determined from the data similar to experiment in (A).

absorption of solar radiation. Since the variation in size allows us to tune the absorption and excited state properties, the obvious question that one might consider is, *How does the size/number of Au atoms in the cluster affect the photocatalytic activity?* If photocatalytic activity in Au_xGSH_y clusters scales with visible absorbance, one would conclude that catalytic activity should scale as $Au_{25}GSH_{18}$ < $Au_{18}GSH_{14}$ < $Au_{15}GSH_{13}$ < $Au_{10-12}GSH_{10-12}$.

Excited Au_xGSH_y clusters are capable of transferring electrons to MV^{2+} and convert it to the reduced form ($MV^{+\bullet}$).[11,39] This photoinduced electron transfer process can be probed using nanosecond laser flash photolysis. Upon reduction of MV^{2+} to $MV^{+\bullet}$, aqueous solutions of methyl viologen change from colorless (Figure 5A) to blue color with absorption peaks at 396 and 605 nm (Figure 5B). Blank experiments carried out with 355 nm laser pulse excitation of a solution containing MV^{2+} and glutathione did not produce any $MV^{+\bullet}$ radicals. Since the yield of $MV^{+\bullet}$ reflects the efficiency of the electron transfer, we can analyze the absorption traces to probe the size-dependent photocatalytic activity of Au_xGSH_y clusters.

In the present study, we probed the $MV^{+\bullet}$ formation at 396 nm (extinction coefficient of 42,100 M^{-1} cm^{-1})[40,41] at different concentrations of MV^{2+}. Figure 6A shows the absorption−time profiles for $Au_{18}GSH_{14}$ solution at different concentrations of MV^{2+}. We averaged the difference absorbance values in the time region of 1.4−1.6 μs (the shaded region in Figure 6A) to determine the concentration of $MV^{+\bullet}$. (Note that the back electron transfer from $MV^{+\bullet}$ to oxidized clusters occurs on a much longer time scale [see Figure S3C in the SI] and hence does not influence the yield at early times.) The triplet excited C_{60} ($^3C_{60}$*) in toluene was employed as an actinometer standard. The Φ_{et} (or quantum efficiency of $MV^{+\bullet}$) was determined using the expression 1.[11,41,42]

$$\Phi_{e-T} = \Phi_T \frac{A_{MV^{2+}} \cdot \varepsilon_{C_{60}}}{A_{C_{60}} \cdot \varepsilon_{MV^{2+}}} \times 100 \quad (1)$$

Φ_T is the quantum yield of $^3C_{60}$* (Φ_T = 1.0), A_{C60} and $A_{MV+\bullet}$ are the maximum absorbance of triplet excited state of C_{60} (at 740 nm) and $MV^{+\bullet}$ (at 396 nm), and ε_{C60} and $\varepsilon_{MV^{+\bullet}}$ are the extinction coefficients of $^3C_{60}$* (ε_{C60} = 12,000 M^{-1} cm^{-1}) and $MV^{+\bullet}$ ($\varepsilon_{MV^{+\bullet}}$ = 42,100 M^{-1} cm^{-1}) at 740 and 396 nm, respectively. The net electron transfer efficiency, Φ_{et} for each of the Au_xGSH_y cluster solutions at different MV^{2+} concentrations was determined by this method, and the results are shown in Figure 6B. The data was collected under equal excitation and with matched absorbance of all solutions at the 355 nm laser

dx.doi.org/10.1021/ja505361n | J. Am. Chem. Soc. 2014, 136, 11093−11099

excitation wavelength. The lifetimes of the transient absorption signal and corresponding Φ_{et} for each of the cluster solutions are summarized in Table 1.

With increasing concentration, more of the excited Au_xGSH_y clusters get quenched (reaction 3), and thus we see an increased yield of $MV^{+\bullet}$. At concentrations greater than 35 μM of MV^{2+} we see a saturation in the yield of $MV^{+\bullet}$, thus indicating the maximum electron transfer yield that we can expect following the excitation of Au_xGSH_y. The $Au_{18}GSH_{14}$ and $Au_{15}GSH_{13}$ clusters exhibit maximum electron transfer yield with a quantum efficiency of ~4%.

$Au_{18}GSH_{14}$ clusters were identified as having the highest potential as photon harvesters due to the high Φ_{et}, as compared with other clusters. While $Au_{15}GSH_{13}$ clusters exhibit a relatively high Φ_{et} (~4%), the total visible photons that can be harvested using these clusters is less than that using $Au_{18}GSH_{14}$ clusters. On the basis of the absorbance, excited state quenching, and electron transfer efficiency we can conclude that $Au_{18}GSH_{14}$ clusters should offer the best photocatalytic performance under solar radiation.

MECHANISM AND RATE CONSTANTS OF QUENCHING BY MV^{2+}

The Φ_{et} discussed in the earlier section represents net electron transfer efficiency following the quenching of the excited gold clusters by MV^{2+}. The reaction scheme for excited state quenching is summarized in reactions 2−5.

$$Au_xGSH_y + h\nu \rightarrow Au_xGSH_y^* \xrightarrow{k_0} Au_xGSH_y \quad (2)$$

$$Au_xGSH_y + MV^{2+} \xrightarrow{k_q} [Au_xGSH_y^{+}\cdots MV^{+\bullet}] \quad (3)$$

$$[Au_xGSH_y^{+}\cdots MV^{+\bullet}] \rightarrow Au_xGSH_y + MV^{2+} \quad (4)$$

$$[Au_xGSH_y^{+}\cdots MV^{+\bullet}] \rightarrow Au_xGSH_y^{+} + MV^{+\bullet} \quad (5)$$

The overall rate constant for quenching of $Au_xGSH_y^*$ is therefore given by k_q. The excited state lifetime of the clusters monitored at ~600 nm (in the absence of MV^{2+}) represents the intrinsic decay rate constant, k_0. On the basis of the decrease in lifetime with increasing MV^{2+} concentration, we determined the quenching rate constant, k_q. The k_q values listed in Table 2 ($k_q \approx 10^{10}$ M^{-1} s^{-1}) show that the encounter between Au_xGSH_y clusters and MV^{2+} is a diffusion-controlled reaction. It is interesting to note that only a fraction of this encounter contributes to net electron transfer (reaction 5). The low electron transfer efficiency listed in Table 1 indicates that the charge recombination within the encounter pair (reaction 4) dominates.

Table 2. Quenching Rate Constants, Quenching Efficiency and Photocatalytic Reduction Yield (η) for Different Metal Clusters

cluster	k_0 (M^{-1} s^{-1})	k_q (M^{-1} s^{-1})	Φ_q (%)	$\eta = \Phi_{et}/\Phi_q$
$Au_{10-12}GSH_{10-12}$	6.1×10^6	1.2×10^{10}	12	0.14
$Au_{15}GSH_{13}$	4.1×10^6	5.4×10^{10}	48	0.08
$Au_{18}GSH_{15}$	3.9×10^6	9.0×10^{10}	62	0.07
$Au_{25}GSH_{18}$	4.9×10^6	6.2×10^{10}	47	0.05

In order to obtain a quantitative estimate of the fraction of excited states quenched by MV^{2+} we determined the quenching efficiency, (Φ_q) for a given MV^{2+} concentration using expression 6.

$$\Phi_q = \frac{k_q[MV^{2+}]}{k_q[MV^{2+}] + k_0} \times 100 \quad (6)$$

The quenching rate constants as well as the fraction of quenching events leading to electron transfer are summarized in Table 2.

The quenching efficiency, Φ_q, varies from 12 to 62% with $Au_{18}GSH_{15}$ clusters exhibiting highest quenching efficiency. A fraction of this quenching results in the net electron transfer efficiency as represented by Φ_{et} in Table 1. By taking the ratio of the two efficiencies (Φ_{et}/Φ_q) we can obtain net photocatalytic electron transfer yield (η) for these four metal clusters. The η values of 0.14 to 0.05 values listed in Table 2 show a decreasing electron transfer yield in the photocatalytic reduction with increasing metal cluster size. The smallest clusters ($Au_{10-12}GSH_{10-12}$) were found to exhibit highest photocatalytic reduction yield (η = 0.14) on the basis of the extent of quenching interaction and to undergo net electron transfer. It should be noted that the Φ_{et} in Table 1 represents net electron transfer efficiency whereas η considers both the quenching efficiency and electron transfer efficiency. The higher quantum efficiency of net electron transfer (Φ_{et}) observed for $Au_{18}GSH_{15}$ clusters in Table 1 can be rationalized from its ability to undergo efficient quenching with MV^{2+}, despite the relatively low fractional quenching events leading to the net electron transfer yield.

CONCLUDING REMARKS

The excited state properties of glutathione-stabilized gold clusters are dependent on the size or number of atoms in the core. The smaller clusters, which are homoleptic complexes, show a long-lived LMCT excited state exclusively, with lifetime in the range of 200 ns. A dominant, rapid relaxation component (τ = ~1 ps) attributed to metal core transitions appears with increasing cluster size. Both $Au_{18}GSH_{14}$ and $Au_{25}GSH_{18}$ exhibit short and longer components in the excited state decay. A long-lived, LMCT state has been identified for each of $Au_{10-12}GSH_{10-12}$, $Au_{15}GSH_{13}$, $Au_{18}GSH_{14}$, and $Au_{25}GSH_{18}$ and is responsible for photocatalytic reduction. The photoactivities of these metal clusters in reducing MV^{2+} show decreasing photocatalytic reduction yield with increasing cluster size. $Au_{18}GSH_{14}$ combines both a high quantum yield for electron transfer and strong visible light absorption, which gives it the highest potential as a sensitizer for light harvesting. Thus, improving effectiveness of metal clusters as a photosensitizer requires maximizing efficiency of quenching, quantum efficiency of electron transfer, and light absorption in the visible. Influencing the LMCT transition through different ligands can further offer opportunities to tune the photosensitizing properties of metal clusters.

ASSOCIATED CONTENT

Supporting Information

Transient absorption (ns and fs) spectra and decay traces for each size of clusters, quenching of excited state lifetimes with MV^{2+} and back electron transfer to clusters, excited state lifetime fittings, excitation intensity dependence of $Au_{25}GSH_{18}$ clusters, and mass spectra analysis. This material is available free of charge via the Internet at http://pubs.acs.org.

dx.doi.org/10.1021/ja505361n | J. Am. Chem. Soc. 2014, 136, 11093−11099

AUTHOR INFORMATION

Corresponding Author

pkamat@nd.edu

Notes

The authors declare no competing financial interest.

ACKNOWLEDGMENTS

The research described herein was supported by the Division of Chemical Sciences, Geosciences and Biosciences, Basic Energy Sciences, Office of Science, U.S. Department of Energy through Grant No. DE-FC02-04ER15533. This is document no. NDRL 5023 from Notre Dame Radiation Laboratory. We would also like to thank the research group of Dr. Xie Jianping for providing the protocols for cluster size analysis and Dr. William Boggess for his assistance in mass spectrometry of clusters at The Mass Spectrometry and Proteomics Facility, University of Notre Dame.

REFERENCES

(1) Devadas, M. S.; Kim, J.; Sinn, E.; Lee, D.; Goodson, T.; Ramakrishna, G. *J. Phys. Chem. C* **2010**, *114*, 22417−22423.
(2) Udayabhaskararao, T.; Pradeep, T. *J. Phys. Chem. Lett.* **2013**, *4*, 1553−1554.
(3) Jin, R.; Qian, H.; Wu, Z.; Zhu, Y.; Zhu, M.; Mohanty, A.; Garg, N. *J. Phys. Chem. Lett.* **2010**, *1* (19), 2903−2910.
(4) Qian, H.; Zhu, M.; Wu, Z.; Jin, R. *Acc. Chem. Res.* **2012**, *45*, 1470−1479.
(5) Kauffman, D. R.; Alfonso, D.; Matranga, C.; Li, G.; Jin, R. *J. Phys. Chem. Lett.* **2012**, *4* (1), 195−202.
(6) Ohta, T.; Shibuta, M.; Tsunoyama, H.; Negishi, Y.; Eguchi, T.; Nakajima, A. *J. Phys. Chem. C* **2013**, *117* (7), 3674−3679.
(7) Yu, Y.; Chen, X.; Yao, Q.; Yu, Y.; Yan, N.; Xie, J. *Chem. Mater.* **2013**, *25*, 946−952.
(8) Yu, Y.; Luo, Z.; Chevrier, D. M.; Leong, D. T.; Zhang, P.; Jiang, D.; Xie, J. *J. Am. Chem. Soc.* **2014**, *136* (4), 1246−9.
(9) Zhu, M.; Aikens, C. M.; Hollander, F. J.; Schatz, G. C.; Jin, R. *J. Am. Chem. Soc.* **2008**, *130* (18), 5883−5.
(10) Tlahuice, A.; Garzón, I. *Phys. Chem. Chem. Phys.* **2012**, *14* (11), 3737.
(11) Stamplecoskie, K. G.; Chen, Y. S.; Kamat, P. V. *J. Phys. Chem. C* **2014**, *118*, 1370−1376.
(12) Philip, R.; Chantharasupawong, P.; Qian, H.; Jin, R.; Thomas, J. *Nano Lett.* **2012**, *12*, 4661−4667.
(13) Das, A.; Li, T.; Nobusada, K.; Zeng, C.; Rosi, N. L.; Jin, R. *J. Am. Chem. Soc.* **2013**, *135*, 18264−18267.
(14) Koivisto, J.; Salorinne, K.; Mustalahti, S. A.; Lahtinen, T.; Malola, S. A.; Hakkinen, H. J.; Pettersson, M. J. *J. Phys. Chem. Lett.* **2014**, *5* (2), 387−392.
(15) Yau, S. H.; Varnavski, O.; Goodson, T. *Acc. Chem. Res.* **2013**, *46* (7), 1506−1516.
(16) Kelly, K. L.; Coronado, E.; Zhao, L. L.; Schatz, G. C. *J. Phys. Chem. B* **2003**, *107*, 668−677.
(17) Aikens, C. M.; Li, S. Z.; Schatz, G. C. *J. Phys. Chem. C* **2008**, *112* (30), 11272−11279.
(18) Chen, M.; Dyer, J. E.; Li, K.; Dixon, D. A. *J. Phys. Chem. A* **2013**, *117* (34), 8298−313.
(19) Chen, Y.; Yang, T.; Pan, H.; Yuan, Y.; Chen, L.; Liu, M.; Zhang, K.; Zhang, S.; Wu, P.; Xu, J. *J. Am. Chem. Soc.* **2014**, *136* (5), 1686−1689.
(20) Stamplecoskie, K. S.; Scaiano, J. C. *J. Am. Chem. Soc.* **2010**, *132* (6), 1825−1827.
(21) Devadas, M.; Kwak, K.; Park, J.; Choi, J.; Jun, C.; Sinn, E.; Ramakrishna, G.; Lee, D. *J. Phys. Chem. Lett.* **2010**, *1* (9), 1497−1503.
(22) Aikens, C. M. *J. Phys. Chem. Lett.* **2011**, *2* (2), 99−104.
(23) Negishi, Y.; Nobusada, K.; Tsukuda, T. *J. Am. Chem. Soc.* **2005**, *127* (14), 5261−5270.
(24) Chen, Y.; Kamat, P. *J. Am. Chem. Soc.* **2014**, *136* (6), 6075−6082.
(25) Chen, Y. S.; Choi, H.; Kamat, P. V. *J. Am. Chem. Soc.* **2013**, *135* (24), 8822−5.
(26) Yu, C.; Li, G.; Kumar, S.; Kawasaki, H.; Jin, R. *J. Phys. Chem. Lett.* **2013**, *4* (17), 2847−2852.
(27) Cha, S.; Kim, J.; Kim, K.; Lee, J. *Chem. Mater.* **2007**, *19*, 6297−6303.
(28) Forward, J. M.; Bohmann, D.; Fackler, J. P.; Staples, R. J. *Inorg. Chem.* **1995**, *34*, 6330−6336.
(29) Jiang, D.; Overbury, S. H.; Dai, S. *J. Am. Chem. Soc.* **2013**, *135*, 8786−8789.
(30) Luo, Z.; Yuan, X.; Yu, Y.; Zhang, Q.; Leong, D. T.; Lee, J. Y.; Xie, J. *J. Am. Chem. Soc.* **2012**, *134*, 16662−16670.
(31) Tlahuice-Flores, A.; Whetten, R. L.; Jose-Yacaman, M. *J. Phys. Chem. C* **2013**, *117*, 20867−20875.
(32) Qian, H.; Sfeir, M. Y.; Jin, R. *J. Phys. Chem. C* **2010**, *114*, 19935−19940.
(33) Smith, B. A.; Zhang, J. Z.; Giebel, U.; Schmid, G. *Chem. Phys. Lett.* **1997**, *270* (1−2), 139−144.
(34) Eustis, S.; El-Sayed, M. *Chem. Soc. Rev.* **2006**, *35* (3), 209−217.
(35) Aruda, K.; Tagliazucchi, M.; Sweeney, C.; Hannah, D.; Schatz, G.; Weiss, E. *Proc. Natl. Acad. Sci. U.S.A.* **2013**, *110* (11), 4212−4217.
(36) Hartland, G. V. *Chem. Rev.* **2011**, *111* (6), 3858−3887.
(37) Link, S.; Burda, C.; Wang, Z. L.; El-Sayeda, M. A. *J. Chem. Phys.* **1999**, *111* (3), 1255−1264.
(38) Mohamed, M. B.; Ahmadi, T. S.; Link, S.; Braun, M.; El-Sayed, M. A. *Chem. Phys. Lett.* **2001**, *343* (1−2), 55−63.
(39) Chen, W.; Hsu, Y.; Kamat, P. V. *J. Phys. Chem. Lett.* **2012**, *3*, 2493−2499.
(40) Peon, J.; Tan, X.; Hoerner, J. D.; Xia, C.; Luk, Y. F.; Kohler, B. *J. Phys. Chem. A* **2001**, *105*, 5768−5777.
(41) Watanabe, T.; Honda, K. *J. Phys. Chem.* **1982**, *86*, 2617−2619.
(42) Dimitrijevic, N. M.; Kamat, P. V. *J. Phys. Chem.* **1992**, *96* (12), 4811−4814.